Published in final edited form as:
Mol Cell Neurosci. 2010 April ; 43(4): 341–352. doi:10.1016/j.mcn.2010.01.001.

Regulation of Synaptic Structure and Function by Palmitoylated AMPA Receptor Binding Protein

Charu Misra[1], **Sophie Restituito**, **Jainne Ferreira**, **Gerald A. Rameau**[2], **Jie Fu**[3], and **Edward B. Ziff**[4]
Department of Biochemistry, New York University School of Medicine, 550 First Avenue, New York, NY 10016.

Abstract

AMPA receptor binding protein (ABP) is a multi-PDZ domain scaffold that binds and stabilizes AMPA receptor (AMPAR) GluR2/3 subunits at synapses. A palmitoylated N-terminal splice variant (pABP-L) concentrates in spine heads, whereas a non-palmitoylated form (ABP-L) is intracellular. We show that postsynaptic sindbisviral expression of pABP-L increased AMPAR mediated mEPSC amplitude and frequency and elevated surface levels of GluR1 and GluR2, suggesting an increase in AMPA receptors at individual synapses. Spines were enlarged and more numerous and nerve terminals contacting these cells displayed enlarged synaptophysin puncta. A non-palmitoylated pABP-L mutant (C11A) did not change spine density or size. Exogenous pABP-L and endogenous GRIP, a related scaffold, colocalized with NPRAP (δ-catenin), to which ABP and GRIP bind, and with cadherins, which bind NPRAP. Thus postsynaptic pABP-L induces pre and postsynaptic changes that are dependent on palmitoylation and likely achieved through ABP association with a multi-molecular cell surface signaling complex.

Keywords

palmitoylation; AMPA receptor; postsynaptic density; ABP; GRIP; spines

Introduction

AMPA receptors are hetero-tetrameric combinations of GluR1-4 subunits that provide the major fast excitatory inputs in the CNS (Hollmann and Heinemann, 1994; Rosenmund et al., 1998). Regulation of AMPA receptor number at the post synaptic membrane contributes to changes in synapse strength and to synaptic plasticity (Barry and Ziff, 2002; Bredt and Nicoll, 2003; Malinow and Malenka, 2002; Sheng and Hyoung Lee, 2003). Such regulation requires a synaptic infrastructure that controls the trafficking and localization of receptors, such as through the interaction of receptors with synaptic scaffolding proteins.

[4] Corresponding author: (E.B. Ziff). Correspondence should be addressed to: Dr Edward B. Ziff, Department of Biochemistry, New York University School of Medicine, 550 First Avenue, New York, NY 10016. Tel: (212) 263 5774, Fax +1 212 263 8214. edward.ziff@nyumc.org.
[1]Present address: Schering Plough Research Institute, 2000 Galloping Hill Road, Kenilworth, NJ 07033
[2]Present address: Dept. of Biology, Morgan State University, 1700 E. Cold Spring Lane, Baltimore MD 21251.
[3]Present address: The City of New York Department of Health, 455 First Avenue, New York, NY 10016

The extreme C-termini of the GluR2 and GluR3 subunits are host to interactions with three PDZ (postsynaptic density-95/ discs large/zona occludens) domain-containing proteins: ABP (AMPA receptor Binding Protein) (Srivastava et al., 1998), PICK1 (Protein Interacting with C Kinase) (Dev et al., 1999; Xia et al., 1999) and GRIP (Glutamate Receptor Interacting Protein) (Dong et al., 1997). Two isoforms of ABP have been cloned: a six (ABP-S) PDZ domain-containing form, and a seven (ABP-L) PDZ containing variant, both of which interact with GluR2 through their fifth PDZ domain (Srivastava et al., 1998). PDZ domain six of ABP binds to liprin-α (Wyszynski et al., 2002), as well as to Eph receptor tyrosine kinases and ephrin ligands (Torres et al., 1998). This provides ABP with the capacity to link AMPA receptors to a large complex of proteins that function in receptor trafficking or synapse modification. ABP-L is substantially homologous to GRIP and whilst their expression overlaps in many CNS neurons, they are also independently expressed (Burette et al., 2001). A variant of ABP-L differing in its first 18 amino acids and exhibiting palmitoylation of the cysteine residue at position 11 has been described (pABP-L), as has a palmitoylated GRIP variant (Yamazaki et al., 2001). pABP-L targets specifically to spine heads, localizing with exogenous GluR2 (DeSouza et al., 2002). The non-palmitoylated variant, ABP-L, is conspicuously absent in spines when exogenously expressed and targets to intracellular clusters, where it partially localizes with exogenous GluR2 at intracellular membranes (DeSouza et al., 2002; Fu et al., 2003). ABP-L PDZ 2 can interact with the ARM domain protein, NPRAP/δ-catenin (Ochiishi et al., 2008; Silverman et al., 2007), which interacts with the synaptic cell adhesion proteins, the cadherins (Lu et al., 1999). The ABP-L complex with NPRAP is directed to the plasma membrane by the cadherin interaction. Dominant negative constructs that disrupt the NPRAP-ABP interaction, decrease the levels of GluR2 at the plasma membrane (Ochiishi et al., 2008; Silverman et al., 2007), confirming the role of this interaction in plasma membrane targeting of GluR1 and GluR2.

Disruption of the GluR2-ABP/GRIP interaction by phosphorylation of the PDZ binding site in the GluR2 C-terminal domain impairs AMPA receptor clustering, increases the rate of GluR2 endocytosis and generates LTD (Chung et al., 2003; Kim et al., 2001; Lu and Ziff, 2005; Matsuda et al., 2000; Osten et al., 2000; States et al., 2008). The trafficking destination of endocytosed GluR2 is not firmly established (States et al., 2008), but several studies suggest a role for ABP/GRIP in tethering AMPARs intracellularly (Daw et al., 2000; Fu et al., 2003).

Although functions for ABP in receptor anchoring and stabilization on the cell surface and intracellularly have been proposed, the roles of the different ABP isoforms in receptor tethering or synaptic function is not known. Also unclear is the significance of the observation that palmitoylation selectively targets and enriches pABP-L in spines (DeSouza et al., 2002), critical structures at which most excitatory synapses in the brain are found (Nimchinsky et al., 2002).

Here, we have expressed exogenous GFP-tagged versions of ABP in hippocampal neurons to gain insights into their functions. We demonstrate that pABP-L expression selectively induces multiple changes relative to ABP-L, including enhancement of synaptic transmission and increase of AMPA receptor abundance at synapses, as well as pre- and post-synaptic development. We also show that ABP/GRIP colocalize with cadherin and NPRAP at synapses. These observations suggest a role for pABP-L, which is localized at the plasma membrane, in establishment and control of synaptic function. Because similar observations have been made for other scaffolds (El-Husseini Ael et al., 2002; Sala et al., 2001; Schluter et al., 2006; Waites et al., 2009), these functions may be more general.

Results

pABP-L expression increases mEPSC frequency and amplitude

To study the roles of pABP-L and ABP-L in synaptic function, we expressed the proteins tagged at the C-terminus with GFP from sindbis virus vectors in cultured hippocampal neurons at DIV 18-21. Fig. 1A shows a schematic representation of the structures of the proteins used in this study. Expression of pABP-L-GFP (henceforth pABP-L) or ABP-L-GFP (henceforth ABP-L) resulted in the formation of puncta that were localized to spines and intracellular clusters respectively (Fig. 1B), as previously described (DeSouza et al., 2002).

Whole-cell recordings were made from pABP-L or ABP-L infected hippocampal neurons, 18 – 25 hours after infection. Recordings were made from infected pyramidal-shaped neurons of similar size. Miniature excitatory post-synaptic currents (mEPSC's) were isolated in the presence of tetrodotoxin to inhibit action potential evoked events. Fig. 1C shows representative mEPSC traces at a holding potential of −70 mV, from pABP-L and ABP-L infected neurons. The downward deflections depict individual miniature synaptic currents. mEPSC's in pABP-L and ABP-L infected neurons were compared with those from uninfected neurons or GFP infected neurons. Mean mEPSC frequencies in GFP infected neurons (1.3 ± 0.4 Hz, $n = 6$) were not significantly different from those in uninfected neurons (0.91 ± 0.2 Hz, $n = 7$), and were subsequently pooled and deemed as controls (mean frequency 1.0 ± 0.2 Hz ($n = 13$)). pABP-L infected neurons displayed an approximate four-fold increase in mEPSC frequency to 5.56 ± 1 Hz, ($n = 7$; range 3.6 – 10.3 Hz). In contrast, ABP-L infected neurons displayed mEPSC frequencies that were similar to those in control cells (1.39 ± 0.3 Hz, $n = 9$); note greater frequency of downward deflections in mEPSC traces for pABP-L compared to ABP-L infected neurons (Fig. 1C). This difference persisted at different holding potentials (data not shown). Further, mEPSCs in neurons overexpressing either pABP-L or ABP-L could be inhibited by CNQX at a holding potential of −70 mV, confirming they were AMPAR mediated (Fig. 1C; $n = 5$ each). Fig. 1D shows data from a number of cells in the form of a bar graph ($p < 0.05$).

We next analyzed the amplitude of mEPSC's from infected neurons. Fig. 1E shows amplitude histograms from an individual pABP-L and ABP-L infected cell. There was a greater distribution of high amplitude events in the pABP-L infected cell (grey, background histogram), than the ABP-L infected cell (blue, forefront histogram). On average, pABP-L infected neurons displayed higher mean amplitude of mEPSCs (−65.1 ± 4 pA), than ABP-L (−51 ± 4 pA) or GFP (−41 ± 5 pA) infected neurons ($p < 0.05$, $n = 8$, 13 and 12 respectively). Fig. 1F shows the scatter of the data, from a number of cells for pABP-L, ABP-L and GFP infected neurons; a significant difference in the amplitude of mEPSCs in pABP-L expressing cells was observed.

These data suggest that pABP-L plays a role in the regulation of synaptic transmission. Since one interpretation of changes in frequency involves changes in quantal release (Murthy et al., 1997) we asked whether there were any changes in the presynaptic terminal subsequent to postsynaptic overexpression of pABP-L.

Large synaptophysin puncta contact pABP-L expressing neurons

We assayed for the effects pABP-L or ABP-L expression on the levels of synaptophysin, a vesicle associate protein used as a presynaptic marker. We stained for synaptophysin at 18 hours after infection, the same time at which electrophysiological recordings were made. Synaptophysin staining was measured in puncta associated with dendrites of neurons expressing the exogenous ABP. These synaptophysin puncta lie within axons that are presynaptic to the neuron expressing the exogenous ABP and do not reside in the same

neuron as the exogenously expressed ABP. Synaptophysin staining density associated with pABP-L expression was markedly greater than the intensity associated with ABP-L infected neurons (Fig. 2A, B, right panels). Synaptophysin staining of puncta proximal to nearby uninfected cells (controls) is shown in the left panels of Fig. 2, for comparison. Synaptophysin staining associated with pABP-L infected neurons was 149.3 ± 14.5 % of control ($p < 0.05$; $n = 4$; 24 cells) and that associated with ABP-L infected neurons, 110 ± 10 % of control ($p > 0.05$; $n = 4$; 24 cells). We also investigated whether there was a difference in the number or size of the associated synaptophysin puncta for pABP-L versus ABP-L infected neurons. A 20 μm length of primary dendrite was selected and the number of synaptophysin puncta contacting the dendrite was counted. Also quantified was the number of synaptophysin puncta with a diameter greater than 1 μm. Whereas the number of synaptophysin puncta contacting infected neurons per 20 μm length of dendrite was not significantly different between pABP-L, ABP-L and GFP infected neurons (15 ± 1.1 puncta, 12.7 ± 1.2 puncta and 12.1 ± 1.7 puncta respectively; $n = 4$; 24 cells), the number of puncta with a diameter greater than 1 μm was significantly more numerous in pABP-L infected neurons (2.74 ± 0.4; $p < 0.05$) than in ABP-L (0.66 ± 0.2) or GFP in fected neurons (0.78 ± 0.3). The mean synaptophysin puncta diameter was: 0.83 ± 0.1, for pABP-L (n = 15) and 0.55 ± 0.06 for ABP-L (n= 12). Fig. 2A depicts this difference indicating the larger and more intense synaptophysin puncta in pABP-L infected neurons; Fig. 2C shows the average data from the synaptophysin experiments in the form of a bar graph. Taken together, these observations suggest that pABP-L infected neurons are contacted by presynaptic terminals with a larger synaptophysin content, which is consistent with the electrophysiological data that demonstrates increased mEPSC frequency.

Surface AMPA receptor abundance increases in pABP-L expressing neurons

While changes in mEPSC frequency often have a presynaptic basis, the results thus far do not exclude a post-synaptic component to the increased mEPSC frequency in pABP-L infected neurons, arising from the insertion of receptors into synapses could not be excluded. Furthermore, ABP plays a role in retaining AMPA receptors at the neuron surface (Kim et al., 2001; Ochiishi et al., 2008; Osten et al., 2000; Perez et al., 2001; Silverman et al., 2007; Xia et al., 1999) and at intracellular sites (Braithwaite et al., 2002; Daw et al., 2000; Fu et al., 2003). We therefore wondered whether overexpression of its isoforms could affect surface AMPA receptor abundance.

We assayed for changes in the surface levels of endogenous GluR2 using a N-terminal monoclonal antibody. Previous studies have demonstrated the co-localization of pABP-L and ABP-L with exogenous Myc-tagged GluR2 pools, both intracellularly and at the plasma membrane (DeSouza et al., 2002; Fu et al., 2003). pABP-L colocalized well with endogenous GluR2, and was abundantly found in spines (Fig. 3A, left panel). In contrast, ABP-L and GluR2 expression overlapped partially at intracellular sites, but not within spines. This is shown in the magnifications of the middle panel in Fig. 3A; arrows indicate the selective expression of GluR2 but not ABP-L in spines. GFP was more diffuse and also colocalized with spines (right panel). The total surface levels of GluR2 were quantified and found to be significantly greater in pABP-L infected neurons than in ABP-L or GFP infected cells ($p < 0.05$). This is shown in the magnifications in Fig. 3A, which highlight a greater intensity of GluR2 staining in pABP-L infected cells than ABPL or GFP infected neurons. Our mean data indicated that there was a 107% increase from control in surface GluR2 levels in pABP-L expressing neurons ($p < 0.05$). In contrast a 22% increase was seen in ABP-L infected neurons, which was not significantly different from controls ($p > 0.05$). The bar graph in Fig. 3B shows our averaged data ($n = 3$, 17 cells). We also quantified the levels of endogenous GluR2 at the surface within individual spines. 10 μm regions of dendrites were isolated and a box of a defined area was drawn around individual spines within these

regions. The levels of GluR2 within this region were then estimated. Similar to the results with the total surface GluR2, we observed a large increase in the total GluR2 intensity in pABP-L infected spines (*n*= 17 cells; 107 spines) when compared with GFP infected neurons (*n*= 14 cells; 75 spines). GluR2 levels in pABP-L infected spines were on average 97 % greater than GluR2 staining in GFP infected cells (see bar graph Fig. 3D). This value correlated well with the increase in surface GluR2 levels observed for the whole cell in pABP-L infected neurons.

We also quantified changes in the levels of GluR1 in ABP infected neurons. Although ABP does not bind to GluR1, we wondered whether surface expression of this subunit was upregulated since AMPA receptors in hippocampal neurons are expressed as heteromers of GluR1/2 as well as GluR2/3. GluR1 staining co-localized well with pABP-L in neurons and both were readily detected in spines as shown in Fig. 4A. There was a 118% increase in surface GluR1 levels as a consequence of pABP-L infection relative to a control expressing GFP ($p < 0.05$) (Fig. 4D). The extent of the increase in surface GluR1 levels following overexpression of pABP-L was almost identical to that observed with GluR2. The increase induced by pABP-L was significantly different from the situation for ABP-L, where only a 22 % increase ($p < 0.05$) in surface GluR1 levels was seen and the level was similar to control neurons expressing GFP (Fig. 4D). As shown in Fig. 4B, GluR1 staining did not colocalize with ABP-L in spines. GFP was expressed throughout the dendrite as expected and its localization did not reflect that of GluR1 (Fig. 4C). These observations are consistent with the view that pABP-L can influence the number of surface AMPA receptors and occupy the same surface compartment, and suggests that a postsynaptic component arising from the insertion of receptors into synapses may also contribute to the increased mEPSC frequency.

Given the enhanced number of surface AMPA receptors in pABP-L expressing cells, we wondered whether there were any postsynaptic morphological changes to accommodate this increase in AMPA receptor density. Indeed, increased AMPA receptor density is correlated with increased spine size (Matsuzaki et al., 2001; Terashima et al., 2004). Other studies have demonstrated changes in spine size following overexpression of various postsynaptic proteins (El-Husseini et al., 2000; Passafaro et al., 2003; Penzes et al., 2001; Rumbaugh et al., 2003; Sala et al., 2001). We therefore asked whether overexpression of pABP-L resulted in any changes in spine morphology.

pABP-L over-expression promotes spine maturation and formation

To assess the effect of pABP-L expression on spine morphology, we compared spines in pABP-L expressing neurons with those in GFP expressing neurons. pABP-L expressing neurons displayed a much higher density of spines than the GFP control (Fig. 5A, B). pABP-L is palmitoylated on cysteine C11 (Fig. 1A). To determine the role of C11 palmitoylation in the spine inducing functions of pABP-L, we infected neurons with C11A-FLAG (henceforth C11A), a non-palmitoylable pABP-L point mutant (Fig. 1A). The number of spines in C11A infected neurons was similar to those in GFP (control) (Fig. 5B, C). In order to quantify these effects, we isolated a 20 μm region on a proximal branch point of the primary dendrite for analysis. We counted the number of clearly visible protrusions from the dendritic shaft within this area. On average there were 13.8 ± 1 spines per 20 μm of dendrite in pABP-L infected neurons (n = 3, 28 cells, 387 spines), 6.7 ± 0.7 spines per 20 μm in GFP infected cells (n = 3, 18 cells, 120 spines) and 5.9 ± 0.4 spines per 20 μm in C11A mutant expressing neurons (n = 3, 28 cells, 164 spines; Fig. 5D). The difference between the numbers of spines in pABP-L neurons compared to C11A or control neurons was significant (T-test, unpaired $p < 0.00001$). There was no significant difference in the number of spines between GFP and C11A infected neurons ($p > 0.05$).

In addition to these effects on spine number, we observed differences in spine morphology. Neurons infected with pABP-L displayed spines with large heads on short, stubby necks in close apposition to the dendritic shaft (mushroom spines; Fig. 5A, bottom panel). On the other hand, control GFP neurons exhibited some mushroom spines (with small heads) and some spines with small heads at the end of long filopodia type shanks (Fig. 5B, bottom panel). Filopodial type spines were conspicuously absent in pABP-L neurons (Fig. 5A). Neurons over-expressing C11A displayed spines similar to those in the GFP control (Fig. 5C). To quantify these effects on spine length and spine head size, we measured the length of individual spines and the number of spines with heads larger than 1 μm within the same analysis region from which density measurements were made. There were 3.9 ± 0.5 large head spines in pABP-L in fected neurons. The comparable value in GFP expressing cells was 0.7 ± 0.2 spines ($p < 0.05$) and 1.2 ± 0.2 in C11A infected neurons (Fig. 5E). The mean spine head diameter was 0.89 ± 0.21 for pABP-L, 0.62 ± 0.16 for GFP and 0.65 ± 0.2 for C11A. pABP-L over-expressing neurons displayed a mean length of spines of 1 ± 0.05 μm (387 spines). This was significantly different from the length of spines in GFP expressing neurons 1.8 ± 0.2 μm (120 spines; $p < 0.001$) and C11A expressing cells (1.5 ± 0.2 μm; 164 spines; $p < 0.01$) and was consistent with the presence of longer spines in GFP expressing neurons (Fig. 5F). The length of spines in C11A cells was not significantly different from control ($p > 0.05$). We also controlled for the ability of GFP staining and C11A staining to analyze spines similarly. In neurons in which GFP was co-infected with C11A (to outline spine morphology clearly) (Fig. 5G), we observed spine density and properties similar to those observed with the C11A mutant alone. In doubly infected C11A-flag and GFP neurons (Fig. 5G), the number of green GFP spines (6.7 ± 1.2) and red C11A spines (6.8 ± 1.3)were similar. This was similar to the number of C11A spines observed in singly infected C11A neurons described above (5.9 ± 0.4), confirming the suitability of C11A staining for spine analysis. The increases in spine number and size observed with pABPL expression are reminiscent of those observed following expression of PSD-95 or of GluR2 (El-Husseini et al., 2000;Passafaro et al., 2003) (Saglietti et al., 2007). Taken together, these observations demonstrate that pABP-L can influence the size, length and number of spines in cultured hippocampal neurons. Because the C11A mutation largely eliminated these influences, the morphological effects of pABP-L depend on palmitoylation of the pABP-L N-terminal domain. Indeed, as seen previously (DeSouza et al., 2002), the levels of C11A in spines were greatly reduced. The low levels of C11A still observed at synapses could reflect the ability of C11A to associate with synaptic structures by a mechanism apart from palmitoylation, such as dimerization with ABP anchored to NPRAP (Silverman et al., 2007) or association with a synaptic target through an N-terminal leader-specific mechanism not dependent on palmitoylation (DeSouza et al., 2002;Silverman et al., 2007).

Colocalization of endogenous GRIP and exogenous pABL-L with NPRAP and cadherin

Cadherins are involved in remodeling of synapses and in maintenance of synaptic function and play a role in synaptic plasticity (Takeichi and Abe, 2005). We previously showed that GluR2 and cadherins could form a complex through the GluR2/3-ABP/GRIP-NPRAP-cadherin interaction (Silverman et al., 2007). In order to understand better the mechanism by which ABP modify spines, we asked if cadherin and NPRAP could colocalize with endogenous and overexpressed ABP or GRIP at synapses.

We first assayed whether endogenous ABP colocalized with cadherin and NPRAP (Fig.6). Because attempts to assay endogenous ABP in cultured neurons using available ABP antibodies yielded low signals, the highly homologous GRIP protein was examined instead. In cultured hippocampal neurons, endogenous GRIP colocalized with NPRAP at synapses (Fig. 6A), as we showed previously (Silverman et al., 2007) and also with cadherin at synapses (Fig. 6B). Moreover exogenous pABP-L also colocalized with NPRAP and

cadherin at synapses (Fig. 6C, D). These data suggest a possible mechanism of AMPAR tethering and spine remodeling through the complex GluR2/3-ABP/GRIP-NPRAP-cadherin.

Discussion

We have shown that postsynaptic expression of pABP-L induces dramatic preand postsynaptic changes. These changes include increased surface AMPA receptor abundance and synaptic strength and were accompanied by structural changes in the presynaptic compartment, increased size of nerve terminals contacting pABP-L expressing cells. Changes were also seen in the postsynaptic compartment, increases in spine size and number. This suggests the existence of a post- to presynaptic signaling mechanism that enables the nerve terminal to respond to pABP-L at the opposing postsynaptic membrane. The changes in spine size and number require pABP-L protein located at the postsynaptic membrane, since a mutation that blocks ABP palmitoylation eliminates the effects on spines. Palmitoylation of ABP directs the protein to spine heads (DeSouza et al., 2002) as also reported for PSD-95 (El-Husseini et al., 2000). Interestingly, PSD-95 induces synaptic changes similar to those reported here for pABPL (El-Husseini et al., 2000).

Overexpression of pABP-L increases synaptic strength

Expression of pABP-L caused an increase in mEPSC amplitude and frequency. The increase in mEPSC amplitude is consistent with the addition of AMPA receptors to individual synapses. This is supported by our observation of increased surface GluR1 and GluR2 in pABP-L expressing neurons. Increases in mEPSC frequency may be ascribed to an increase in the presynaptic release of quanta (Murthy et al., 1997), or to the delivery of AMPA receptors to synapses (Isaac et al., 1995; Liao et al., 1995) or to change in mEPSC amplitude detection levels. The enhanced size of axon terminals contacting neurons expressing pABP-L suggests that an increased probability of release associated with a larger vesicle pool size could account for the increase in mEPSC frequency.

Overexpression of the scaffolding proteins, PSD-95 and SHANK, also increase mEPSC frequency, through an enhancement of presynaptic release in hippocampal neurons (El-Husseini et al., 2000; Sala et al., 2001). However, since we also observed an increase in surface AMPA receptor levels, the insertion of AMPA receptors into synapses may contribute a postsynaptic aspect to the increased mEPSC frequency. It is unlikely that the change in mEPSC frequency is secondary to a change in mEPSC amplitude detection levels (if the amplitude increases, more mEPSCs become detectable) since we also observed the increased frequency at lower holding potentials (data not shown). These findings are consistent with previous studies that suggest a role for the GluR2-ABP/GRIP interaction in modulating synaptic transmission (Daw et al., 2000; Kim et al., 2001; Matsuda et al., 2000; Silverman et al., 2007).

The role of pABP-L in postsynaptic enhancement

We find that overexpression of pABP-L increases endogenous surface GluR2 within neurons and individual spines. This is consistent with a role for ABP in the stabilization of GluR2 at the plasma membrane (Ochiishi et al., 2008; Osten et al., 2000; Seidenman et al., 2003; Silverman et al., 2007) and suggests that the abundance of pABPL at the surface may be a key determinant of AMPA receptor density. The increase in surface endogenous GluR1 levels may seem anomalous, since GluR1 does not bind directly to ABP (Srivastava et al., 1998). However, since GluR1 homomers are sparse in the hippocampus (Wenthold et al., 1996), the most parsimonious interpretation of the increase would be that GluR1 hetero-oligomerizes with GluR2. Indeed, we observed similar increases in the levels of GluR1 and GluR2 subsequent to pABP-L expression. However, other studies have suggested that the

delivery of GluR1/2 heteromers to synaptic sites is regulated by activity (Shi et al., 2001). This leads to the possibility that the increased glutamate release associated with the enlarged presynaptic terminals contacting pABP-L infected neurons provides the *activity* for regulated GluR1 delivery.

The levels of AMPA receptors at the synapse may be determined by the presence of synaptic 'placeholders' or 'slots' for cycling AMPA receptors (Bredt and Nicoll, 2003; Shi et al., 2001). Up or down-regulation of slot numbers during plasticity could control AMPA receptor density (Bredt and Nicoll, 2003; Shi et al., 2001). As such, pABP-L may be a good candidate for a slot protein, since its overexpression increases AMPA receptor abundance and enhances synaptic transmission. How a slot protein function for pABP-L relates to the previously proposed slot proteins remains to be determined (Shi et al., 2001). Overexpression of PSD-95 also positively influences synaptic transmission and AMPA receptor number through PSD-95 association with Stargazin, which binds AMPA receptors (Chetkovich et al., 2002; Schnell et al., 2002).Thus PSD-95 may also fulfill a possible slot protein function (El-Husseini et al., 2000; Sheng and Hyoung Lee, 2003).

In cultured hippocampal neurons, exogenous GluR2 trafficks from the plasma membrane to intracellular ABP-L clusters and colocalizes with these clusters, dependent on PDZ interaction (Burette et al., 2001.; Fu et al., 2003; Wyszynski et al., 1999). This suggests that intracellular ABP can bind and possibly tether AMPA receptors that are in active transport. In the current study, however, overexpression of ABP-L did not diminish surface AMPA receptor number or synaptic transmission as might be expected were ABP-L solely an intracellular AMPA receptor tether. This suggests that elevation of the level of intracellular ABP-L did not create intracellular GluR2 binding sites that competed with sites at the plasma membrane for AMPA receptors leading to a reduction in GluR2 surface levels. Possibly an additional factor beyond the intracellular level of ABP is necessary to generate an intracellular binding site and for a GluR2 AMPA receptor to occupy that site. We note that GluR2 trafficking is regulated by GluR2 C-terminal phosphorylation (Chung et al., 2003; Chung et al., 2000; Lu and Ziff, 2005; Matsuda et al., 2000; Matsuda et al., 1999; Perez et al., 2001), which could play a role in establishing intracellular receptor levels. Further work is required to evaluate the function of intracellular ABP-complexes in determining the population of intracellular AMPA receptors.

Our work shows that an increase in the levels of exogenous ABP-L did not elevate the quantity of AMPA receptors at the plasma membrane. ABP-L can, however occupy a position at the plasma membrane through binding to NPRAP that is associated with cadherins (Silverman et al., 2007), as suggested by the colocalization of ABP/GRIP with NPRAP and cadherin. This in turn suggests a mechanism by which ABP-L, linked via NPRAP to cadherins may have synapse modifying properties similar to pABP-L. Because we have shown that GRIP (and presumably the closely related ABP) colocalizes with NPRAP and cadherin at synapses, it is possible that these synapses are already saturated with ABP-L and the related non-palmitoylated GRIP species. In this case, exogenous expression would not elevate the synaptic levels of these scaffolds or any associated AMPA receptors.

Regulation of spine size and number by pABP-L

During spine maturation, dendritic filopodia shorten upon contact with presynaptic terminals, and pull the spine head closer to the dendrite (Dailey and Smith, 1996). Our observation that overexpression of pABP-L causes an increase in spine number, enlarges the spine head and decreases spine length, therefore suggests that pABP-L enhances spine maturation. The link between spine size and AMPA receptor content (Matsuzaki et al., 2001) is also in accord with our findings of elevated surface AMPA receptors in pABP-L

expressing cells. Since the increases in density and size of spines are greatly reduced with the non-palmitoylated C11A mutant, palmitoylation-dependent synaptic recruitment of pABP-L is critical for the spine-promoting activity. Other postsynaptic proteins, including PSD-95, Kalirin, Rac, SHANK and GluR2, promote similar effects (El-Husseini et al., 2000; Nakayama et al., 2000; Passafaro et al., 2003; Sala et al., 2001).

What mechanisms are likely to contribute to these effects on spines? It seems reasonable to propose that pABP-L stabilizes the GluR2 - pABP-L complex at the surface and may position other factors that induce synaptic changes at the synapse. One such factor is AMPA receptors themselves, since the GluR2 N-terminal extracellular domain interaction with cadherins can induce synaptic maturation of the sort observed for pABPL (Passafaro et al., 2003; Saglietti et al., 2007). ABP binds to complexes of NPRAP/δ-catenin with cadherins, which can in turn tether GluR2 in proximity to cadherins (Silverman et al., 2007), facilitating GluR2-cadherin interaction. Indeed we observed a colocalization of ABP/GRIP with NPRAP and cadherin. The complex of receptors, scaffolds, and adhesion proteins formed by these interactions may stabilize synapse structures, leading to spine maturation. The ephrinB-EphB receptor signaling pair is another candidate for a pABP-L and PSD-95-associated synapse maturation factor that contributes to spine dynamics. This receptor-ligand pair signals both pre and postsynaptically and induces changes in spine morphology (Henkemeyer et al., 2003). ABP can associate directly with Eph receptors and ephrins via its PDZ domains (Torres et al., 1998) and PSD-95 binds indirectly via its complex with the NMDA receptor, which binds EphB receptor, which in turn binds ephrinB (Dalva et al., 2000).

Despite an enlargement in the size of synaptophysin puncta, the number of puncta in contact with individually infected neurons was conserved between pABP-L, ABP-L and GFP overexpressing neurons. This suggests that pABP-L overexpression does not induce presynaptic contacts *de novo* but promotes the enhancement of existing presynaptic terminals. This differs from the effects in the postsynaptic cell, where in addition to enlarging the spine head, pABP-L also induces new spines. In fact, the ratio of spines to synaptophysin puncta increases from 1:2 in GFP infected neurons to 1:1 in pABP-expressing cells. This change may represent the conversion of synapses made directly on the dendrite (axo-dendritic) to those made onto the spine head itself in pABPL expressing cells. Alternatively, spines not previously detected due to their small size may become detectable following enlargement of the spine head in pABP-L expressing cells. Nonetheless, spine maturation by pABP-L almost certainly involves the elaboration of actin filaments, which play a major role in spine morphology. pABP-L may regulate actin indirectly through its association with Eph receptor tyrosine kinases and ephrin ligands (Torres et al., 1998), which activate Kalirin 7, a critical regulator of actin dynamics (Penzes et al., 2003). In addition, ABP could regulate actin through binding to NPRAP/d-catenin (Silverman et al., 2007), which binds cortactin, a factor that promotes actin polymerization (Martinez et al., 2003).

Similarities of the PSD-95/SAP97 and ABP/GRIP families of scaffolds

The scaffolding proteins, PSD-95, SAP97, ABP and GRIP, are components of a large molecular complex that determines structural and functional properties of the synapse. Overexpression of PSD-95 increased synaptic transmission (El-Husseini et al., 2000) in a manner dependent upon the PSD-95 isoform, which differ in the N-terminal domain (Schluter et al., 2006). The PSD-95 α-isoform is palmitoylated at cysteine 3 and 5 and strongly increases synaptic transmission, while the β-isoform, which is not palmitoylated but contains an N-terminal L27 protein interaction sequence, did not increase transmission unless endogenous PSD-95 was knocked down. PSD-95 knockdown decreased transmission, whereupon PSD-95 β-isoform expression restored transmission to control levels, but

transmission did not reach the levels induced by the α-isoform. PSD-95 regulates both synaptic strength and the potential for LTD respectively through its N-terminal and C-terminal sequences (Xu et al., 2008). This suggests that molecular interactions with these PSD-95 domains contribute different functions. Significantly, N-terminal domain phosphorylation by CaMKII releases PSD-95 from the spine and regulates PSD-95's ability to enhance spine growth and potentiate synapses (Steiner et al., 2008). Because the α- and β-isoforms of SAP-97 function similarly to the PSD-95 isoforms, different scaffolds of the MAGUK family are able to potentiate synapses (Schluter et al., 2006).

The closely related ABP and GRIP proteins studied here form a second family of scaffolds distinct from the MAGUKs. Both ABP and GRIP are expressed in palmitoylated and non-palmitoylated isoforms comparable to the α- and β-isoforms of PSD-95 and SAP97. We show that the capacity of these two isoforms to potentiate synapses when overexpressed is similar to that of the two MAGUK proteins. Thus, overexpression of pABP-L increased both electrophysiological and morphological properties of synapses, as did overexpression of the two MAGUK α-isoforms, while the non-palmitoylated form, ABP-L, had no effect, similar to the two MAGUK β-isoforms when they were expressed in the presence of endogenous scaffolds (Schluter et al., 2006). Thus, despite significant structural differences, the MAGUKs and ABP/GRIP can exert similar forms of synapse regulation. We have not determined whether expression of nonpalmitoylated ABP or GRIP would restore transmission properties in neurons following PSD-95 knockdown.

Our study demonstrates that GluR2-PDZ interacting proteins such as pABP-L can positively affect synaptic transmission and can communicate structural plasticity across the synaptic cleft. pABP-L may bring together a group of proteins that modulate synapse functions. By varying levels of synaptic pABP-L, neurons may achieve differential sensitivity to synaptic inputs.

Experimental methods

Cell culture and Sindbis virus infection of hippocampal neurons

Hippocampal primary cultures were prepared from E18 Sprague Dawley rat embryonic tissue by dissociation with trypsin as previously described (Osten et al., 2000). Briefly, dissected hippocampal were triturated and suspended in minimal essential medium containing 1 μM pyruvate, 25 μM glucose, horse serum and antibiotics. The cells were plated onto sterile, poly-L-lysine coated coverslips, in 6-well dishes at a density of 1.2×10^5 cells per well. After 3 hr, the medium was replaced with neurobasal medium supplemented with B27, and maintained for ~ 3 weeks. All media were from Life Technologies (Gibco BRL). AraC was added after 6 days to suppress glial cell growth. Hippocampal neurons were infected for 18 hours, at 18-21 days in vitro (DIV) with 20 μl of virus stock per well of 6-well dish. For electrophysiological experiments, coverslips were transferred to 35 μm cell culture dishes containing recording solution and viewed under the microscope. In general spines were identified as clearly visible protrusions from the dendritic shaft within a defined area. In the initial experiments with the pABP-L mutant C11A, neurons were coinfected with two sindbis viruses expressing C11A and GFP, and spine structure, length and properties were analyzed. In these doubly infected neurons, GFP and C11A had overlapping distributions. Because of the similar distributions, subsequent experiments were conducted on neurons with single C11A sindbis infections.

Electrophysiology and analysis of mini EPSCs Solutions

The external solution contained (mM), NaCl, 140; $CaCl_2$, 2; $MgCl_2$, 5; KCl, 5; HEPES, 25 and Glucose, 33 (adjusted to pH 7.3 with NaOH). The intracellular pipette solution

contained (mM): Kgluconate, 145; NaCl, 8; HEPES, 10; EGTA, 0.2; MgATP, 2; Na_3GTP, 3 and QX314, 5, (pH 7.3). The osmolarity of solutions was ~300 mOsm (VAPRO, vapor pressure osmometer, Wescor). To isolate mini Excitatory Post-Synaptic Currents (mEPSC's), recordings were made in the presence of 500 nM TTX and further supplemented with 20 μM bicuculline methobromide and 1 μM strychnine, to block inhibitory currents. All solutions were bath-applied through a gravity-feed mechanism. In some experiments, 5 μM CNQX was locally applied, through pressure ejection of solution, using a perfusion device (DAD-12, ALA Scientific Instruments, New York). The tip was placed ~ 50 μm from the recorded cell. Drugs were obtained from Sigma, with the exception of bicuculline methobromide (Tocris).

Recording Procedures

Whole-cell recordings were made at room temperature from fluorescent, spindle-shaped hippocampal neurons expressing tagged proteins. Cells were visually identified under a Nikon Diaphot 200 inverted microscope, connected to a mercury lamp. Patch pipettes were pulled from borosilicate glass capillaries (Harvard Apparatus GC150F-10) using a laser-puller (Sutter instruments), coated with Sylgard (Dow Corning 184) and fire-polished to a final resistance of 5 - 8 MΩ. Whole-cell recordings were made from similar sized neurons using an Axopatch 200B amplifier in the voltage-clamp configuration. Capacitance measurements from pABP-L, ABP-L, GFP infected neurons and uninfected cells were 26.7 ± 1.3 pF (n = 29), 27.6 ± 1.2 pF (n = 24), 25.3 ± 2.1 pF (n = 8) and 25.7 ± 0.8 pF (n = 14) respectively and were not significantly different between the groups ($p > 0.05$). Passive cell properties were monitored throughout the recording and cells in which the series resistance changed by greater than 20%, were discarded from analysis. All recordings were stored directly onto a computer, after being filtered at 2 kHz and digitized at 10 kHz (PCLAMP 8, Axon Instruments).

Data Analysis

mEPSC's were identified using NPM044 (Stephen Traynelis, Emory University, Atlanta, GA) and recorded for a period of 5 to 10 minutes, depending on the frequency of events. A minimum of 100 events were analyzed per cell to obtain estimates of frequency and amplitude. In two cells, recordings were interrupted by a capacitive transient measurement. These cells were used to yield estimates of mEPSC amplitude only. Averaged waveforms were constructed by aligning mEPSC's on their rising phase. Current decays were fitted to an exponential waveform using Origin version 6.0. (Microcal, Northampton MA). Cells in which the rise-time of events was greater than 1 ms were discarded from analysis. All values are expressed as means ± s.e.m's and statistical significance between groups was assayed using the Students' paired or unpaired T-Test, and considered significant at the $p < 0.05$.

Immunocytochemistry

All of the Sindbis pseudovirions were generated as described in the Sindbis Expression System manual (Invitrogen). Briefly, BHK cells were electroporated with RNA transcribed *in vitro* from pSinRep5 vectors encoding either pABP-L-GFP or ABPL-GFP and from the helper plasmid DH26S. The medium containing pseudovirions was collected and used for infection as previously described (Osten et al., 2000). Flag-tagged ABP mutant C11A was generated as previously described (DeSouza et al., 2002). For surface staining, live neurons were incubated with 10 μg/ml of anti-GluR1 N-terminal polyclonal antibody (Chemicon) or 10 μg/ml of anti-GluR2 N-terminal monoclonal antibody (Chemicon) for 30 minutes at 37°C. Cells were then briefly washed with 1X PBS and fixed with 4% paraformaldehyde, before being blocked with 3 % Bovine Serum Albumin. Cells were washed and incubated with a 1:200 dilution of rhodamine secondary antibody (Jackson ImmunoResearch, West Grove, PA) and visualized under a confocal microscope (Nikon PCM 2000). For

experiments with synaptophysin, NPRAP and cadherin, cells were washed with 1X PBS, fixed in paraformaldehye (4%), permeabilized (0.2% Triton) and incubated with a 1:300 dilution of mouse anti-synaptophysin (Sigma, St Louis, MO), 1:200 of mouse anti-δ-catenin (BD Biosciences), 1:100 of mouse anti-N-cadherin (BD Biosciences) or 1: 250 of rabbit anti-GRIP (Upstate). The secondary antibody was rhodamine anti-mouse used at a dilution of 1:250. Neurons tagged with FLAG were washed, fixed, blocked and incubated with mouse anti-M2 Flag antibody (Sigma) at a concentration of 0.4 μg/ml. The secondary antibodies were conjugated and from Jackson laboratory or or Alexa probes and used at respectively 1:250 and 1:500. Images were captured with visualized under a confocal microscope (Nikon PCM 2000) or a Zeiss (Thornwood, NY) LSM510 Meta laser-scanning confocal microscope using a Plan-Apochromat 63x objective and LSM 510 Meta software.

Immunostaining data analysis

All images were acquired on a Nikon PCM 2000 Laser Scanning Personal Confocal Microscope using Simple32 C-imaging 128- Image Analysis System. The exposure setting and gain of laser settings were kept the same for each staining, but different between experimental paradigms. To analyze the intensity of the staining of infected neurons, cells of a similar size and number of dendritic branches were selected. The average color intensity was estimated from distribution of pixel intensity values. Quantitation of surface expression for both GluR1 and GluR2 as well as intensity for synaptophysin staining, were based on 3 platings of neurons. Cell soma was excluded from the field of analysis. For quantitation of synaptophysin puncta, number and size, a 20 μm region of primary dendrite was selected, and the number of puncta contacting this region were counted. Within the same region, the number of synaptophysin puncta with a diameter greater than 1 μm (measured in Adobe Photoshop 7), were also counted.

For measurement of spine parameters, a 20 μm region of dendrite was selected and the length (from the dendritic shaft to the furthest point of the spine head), width (two most distant points within the spine head), and number of spines were quantified using Adobe Photoshop 7. Spines were identified, as clear projections from the dendritic shaft. Aggregates of protein close to the shaft periphery were not considered in spine measurements. For measurement of GluR2 levels within spines, a 10 μm region of dendrite, close to the primary dendrite was selected. Individual spines within this region were isolated by boxing them within a 2 μm by 4 μm region. The GluR2 content within these spines was quantified.

Acknowledgments

This work was supported by a grant from the NIH to E.B.Z. (R01AG13620) and by a grant from the Alzheimer's Association to SR (NIRG-06-25401).

We thank Wei Lu for helpful discussions and Wei Lu and Brian Fernholz for critical reading of this manuscript. We are grateful to Laveria Lee and Sunita DeSouza for virus stocks.

References

Barry MF, Ziff EB. Receptor trafficking and the plasticity of excitatory synapses. Curr Opin Neurobiol. 2002; 12:279–286. [PubMed: 12049934]

Braithwaite SP, Xia H, Malenka RC. Differential roles for NSF and GRIP/ABP in AMPA receptor cycling. Proc Natl Acad Sci U S A. 2002; 99:7096–7101. [PubMed: 12011465]

Bredt DS, Nicoll RA. AMPA receptor trafficking at excitatory synapses. Neuron. 2003; 40:361–379. [PubMed: 14556714]

Burette A, Khatri L, Wyszynski M, Sheng M, Ziff EB, Weinberg RJ. Differential cellular and subcellular localization of ampa receptor-binding protein and glutamate receptor-interacting protein. J Neurosci. 2001; 21:495–503. [PubMed: 11160429]

Chetkovich DM, Chen L, Stocker TJ, Nicoll RA, Bredt DS. Phosphorylation of the postsynaptic density-95 (PSD-95)/discs large/zona occludens-1 binding site of stargazin regulates binding to PSD-95 and synaptic targeting of AMPA receptors. J Neurosci. 2002; 22:5791–5796. [PubMed: 12122038]

Chung HJ, Steinberg JP, Huganir RL, Linden DJ. Requirement of AMPA receptor GluR2 phosphorylation for cerebellar long-term depression. Science. 2003; 300:1751–1755. [PubMed: 12805550]

Chung HJ, Xia J, Scannevin RH, Zhang X, Huganir RL. Phosphorylation of the AMPA receptor subunit GluR2 differentially regulates its interaction with PDZ domain-containing proteins. J Neurosci. 2000; 20:7258–7267. [PubMed: 11007883]

Dailey ME, Smith SJ. The dynamics of dendritic structure in developing hippocampal slices. J Neurosci. 1996; 16:2983–2994. [PubMed: 8622128]

Dalva MB, Takasu MA, Lin MZ, Shamah SM, Hu L, Gale NW, Greenberg ME. EphB receptors interact with NMDA receptors and regulate excitatory synapse formation. Cell. 2000; 103:945–956. [PubMed: 11136979]

Daw MI, Chittajallu R, Bortolotto ZA, Dev KK, Duprat F, Henley JM, Collingridge GL, Isaac JT. PDZ proteins interacting with C-terminal GluR2/3 are involved in a PKC-dependent regulation of AMPA receptors at hippocampal synapses. Neuron. 2000; 28:873–886. [PubMed: 11163273]

DeSouza S, Fu J, States BA, Ziff EB. Differential palmitoylation directs the AMPA receptor-binding protein ABP to spines or to intracellular clusters. J Neurosci. 2002; 22:3493–3503. [PubMed: 11978826]

Dev KK, Nishimune A, Henley JM, Nakanishi S. The protein kinase C alpha binding protein PICK1 interacts with short but not long form alternative splice variants of AMPA receptor subunits. Neuropharmacology. 1999; 38:635–644. [PubMed: 10340301]

Dong H, O'Brien RJ, Fung ET, Lanahan AA, Worley PF, Huganir RL. GRIP: a synaptic PDZ domain-containing protein that interacts with AMPA receptors. Nature. 1997; 386:279–284. [PubMed: 9069286]

El-Husseini AE, Schnell E, Chetkovich DM, Nicoll RA, Bredt DS. PSD-95 involvement in maturation of excitatory synapses. Science. 2000; 290:1364–1368. [PubMed: 11082065]

El-Husseini Ael D, Schnell E, Dakoji S, Sweeney N, Zhou Q, Prange O, Gauthier-Campbell C, Aguilera-Moreno A, Nicoll RA, Bredt DS. Synaptic strength regulated by palmitate cycling on PSD-95. Cell. 2002; 108:849–863. [PubMed: 11955437]

Fu J, deSouza S, Ziff EB. Intracellular membrane targeting and suppression of Ser880 phosphorylation of glutamate receptor 2 by the linker I-set II domain of AMPA receptor-binding protein. J Neurosci. 2003; 23:7592–7601. [PubMed: 12930798]

Henkemeyer M, Itkis OS, Ngo M, Hickmott PW, Ethell IM. Multiple EphB receptor tyrosine kinases shape dendritic spines in the hippocampus. J Cell Biol. 2003; 163:1313–1326. [PubMed: 14691139]

Hollmann M, Heinemann S. Cloned glutamate receptors. Annu Rev Neurosci. 1994; 17:31–108. [PubMed: 8210177]

Isaac JT, Nicoll RA, Malenka RC. Evidence for silent synapses: implications for the expression of LTP. Neuron. 1995; 15:427–434. [PubMed: 7646894]

Kim CH, Chung HJ, Lee HK, Huganir RL. Interaction of the AMPA receptor subunit GluR2/3 with PDZ domains regulates hippocampal long-term depression. Proc Natl Acad Sci U S A. 2001; 98:11725–11730. [PubMed: 11573007]

Liao D, Hessler NA, Malinow R. Activation of postsynaptically silent synapses during pairing-induced LTP in CA1 region of hippocampal slice. Nature. 1995; 375:400–404. [PubMed: 7760933]

Lu Q, Paredes M, Medina M, Zhou J, Cavallo R, Peifer M, Orecchio L, Kosik KS. delta-catenin, an adhesive junction-associated protein which promotes cell scattering. J Cell Biol. 1999; 144:519–532. [PubMed: 9971746]

Lu W, Ziff EB. PICK1 interacts with ABP/GRIP to regulate AMPA receptor trafficking. Neuron. 2005; 47:407–421. [PubMed: 16055064]

Malinow R, Malenka RC. AMPA receptor trafficking and synaptic plasticity. Annu Rev Neurosci. 2002; 25:103–126. [PubMed: 12052905]

Martinez MC, Ochiishi T, Majewski M, Kosik KS. Dual regulation of neuronal morphogenesis by a delta-catenin-cortactin complex and Rho. J Cell Biol. 2003; 162:99–111. [PubMed: 12835311]

Matsuda S, Launey T, Mikawa S, Hirai H. Disruption of AMPA receptor GluR2 clusters following long-term depression induction in cerebellar Purkinje neurons. EMBO J. 2000; 19:2765–2774. [PubMed: 10856222]

Matsuda S, Mikawa S, Hirai H. Phosphorylation of serine-880 in GluR2 by protein kinase C prevents its C terminus from binding with glutamate receptor-interacting protein. J Neurochem. 1999; 73:1765–1768. [PubMed: 10501226]

Matsuzaki M, Ellis-Davies GC, Nemoto T, Miyashita Y, Iino M, Kasai H. Dendritic spine geometry is critical for AMPA receptor expression in hippocampal CA1 pyramidal neurons. Nat Neurosci. 2001; 4:1086–1092. [PubMed: 11687814]

Murthy VN, Sejnowski TJ, Stevens CF. Heterogeneous release properties of visualized individual hippocampal synapses. Neuron. 1997; 18:599–612. [PubMed: 9136769]

Nakayama AY, Harms MB, Luo L. Small GTPases Rac and Rho in the maintenance of dendritic spines and branches in hippocampal pyramidal neurons. J Neurosci. 2000; 20:5329–5338. [PubMed: 10884317]

Nimchinsky EA, Sabatini BL, Svoboda K. Structure and function of dendritic spines. Annu Rev Physiol. 2002; 64:313–353. [PubMed: 11826272]

Ochiishi T, Futai K, Okamoto K, Kameyama K, Kosik KS. Regulation of AMPA receptor trafficking by delta-catenin. Mol Cell Neurosci. 2008; 39:499–507. [PubMed: 18602475]

Osten P, Khatri L, Perez JL, Kohr G, Giese G, Daly C, Schulz TW, Wensky A, Lee LM, Ziff EB. Mutagenesis reveals a role for ABP/GRIP binding to GluR2 in synaptic surface accumulation of the AMPA receptor. Neuron. 2000; 27:313–325. [PubMed: 10985351]

Passafaro M, Nakagawa T, Sala C, Sheng M. Induction of dendritic spines by an extracellular domain of AMPA receptor subunit GluR2. Nature. 2003; 424:677–681. [PubMed: 12904794]

Penzes P, Beeser A, Chernoff J, Schiller MR, Eipper BA, Mains RE, Huganir RL. Rapid induction of dendritic spine morphogenesis by trans-synaptic ephrinBEphB receptor activation of the Rho-GEF kalirin. Neuron. 2003; 37:263–274. [PubMed: 12546821]

Penzes P, Johnson RC, Sattler R, Zhang X, Huganir RL, Kambampati V, Mains RE, Eipper BA. The neuronal Rho-GEF Kalirin-7 interacts with PDZ domain-containing proteins and regulates dendritic morphogenesis. Neuron. 2001; 29:229–242. [PubMed: 11182094]

Perez JL, Khatri L, Chang C, Srivastava S, Osten P, Ziff EB. PICK1 targets activated protein kinase Calpha to AMPA receptor clusters in spines of hippocampal neurons and reduces surface levels of the AMPA-type glutamate receptor subunit 2. J Neurosci. 2001; 21:5417–5428. [PubMed: 11466413]

Rosenmund C, Stern-Bach Y, Stevens CF. The tetrameric structure of a glutamate receptor channel. Science. 1998; 280:1596–1599. [PubMed: 9616121]

Rumbaugh G, Sia GM, Garner CC, Huganir RL. Synapse-associated protein-97 isoform-specific regulation of surface AMPA receptors and synaptic function in cultured neurons. J Neurosci. 2003; 23:4567–4576. [PubMed: 12805297]

Saglietti L, Dequidt C, Kamieniarz K, Rousset MC, Valnegri P, Thoumine O, Beretta F, Fagni L, Choquet D, Sala C, Sheng M, Passafaro M. Extracellular interactions between GluR2 and N-cadherin in spine regulation. Neuron. 2007; 54:461–477. [PubMed: 17481398]

Sala C, Piech V, Wilson NR, Passafaro M, Liu G, Sheng M. Regulation of dendritic spine morphology and synaptic function by Shank and Homer. Neuron. 2001; 31:115–130. [PubMed: 11498055]

Schluter OM, Xu W, Malenka RC. Alternative N-terminal domains of PSD-95 and SAP97 govern activity-dependent regulation of synaptic AMPA receptor function. Neuron. 2006; 51:99–111. [PubMed: 16815335]

Schnell E, Sizemore M, Karimzadegan S, Chen L, Bredt DS, Nicoll RA. Direct interactions between PSD-95 and stargazin control synaptic AMPA receptor number. Proc Natl Acad Sci U S A. 2002; 99:13902–13907. [PubMed: 12359873]

Seidenman KJ, Steinberg JP, Huganir R, Malinow R. Glutamate receptor subunit 2 Serine 880 phosphorylation modulates synaptic transmission and mediates plasticity in CA1 pyramidal cells. J Neurosci. 2003; 23:9220–9228. [PubMed: 14534256]

Sheng M, Hyoung Lee S. AMPA receptor trafficking and synaptic plasticity: major unanswered questions. Neurosci Res. 2003; 46:127–134. [PubMed: 12767475]

Shi S, Hayashi Y, Esteban JA, Malinow R. Subunit-specific rules governing AMPA receptor trafficking to synapses in hippocampal pyramidal neurons. Cell. 2001; 105:331–343. [PubMed: 11348590]

Silverman JB, Restituito S, Lu W, Lee-Edwards L, Khatri L, Ziff EB. Synaptic anchorage of AMPA receptors by cadherins through neural plakophilin-related arm protein AMPA receptor-binding protein complexes. J Neurosci. 2007; 27:8505–8516. [PubMed: 17687028]

Srivastava S, Osten P, Vilim FS, Khatri L, Inman G, States B, Daly C, DeSouza S, Abagyan R, Valtschanoff JG, Weinberg RJ, Ziff EB. Novel anchorage of GluR2/3 to the postsynaptic density by the AMPA receptor-binding protein ABP. Neuron. 1998; 21:581–591. [PubMed: 9768844]

States BA, Khatri L, Ziff EB. Stable synaptic retention of serine-880-phosphorylated GluR2 in hippocampal neurons. Mol Cell Neurosci. 2008; 38:189–202. [PubMed: 18417360]

Steiner P, Higley MJ, Xu W, Czervionke BL, Malenka RC, Sabatini BL. Destabilization of the postsynaptic density by PSD-95 serine 73 phosphorylation inhibits spine growth and synaptic plasticity. Neuron. 2008; 60:788–802. [PubMed: 19081375]

Takeichi M, Abe K. Synaptic contact dynamics controlled by cadherin and catenins. Trends Cell Biol. 2005; 15:216–221. [PubMed: 15817378]

Terashima A, Cotton L, Dev KK, Meyer G, Zaman S, Duprat F, Henley JM, Collingridge GL, Isaac JT. Regulation of synaptic strength and AMPA receptor subunit composition by PICK1. J Neurosci. 2004; 24:5381–5390. [PubMed: 15190111]

Torres R, Firestein BL, Dong H, Staudinger J, Olson EN, Huganir RL, Bredt DS, Gale NW, Yancopoulos GD. PDZ proteins bind, cluster, and synaptically colocalize with Eph receptors and their ephrin ligands. Neuron. 1998; 21:1453–1463. [PubMed: 9883737]

Waites CL, Specht CG, Hartel K, Leal-Ortiz S, Genoux D, Li D, Drisdel RC, Jeyifous O, Cheyne JE, Green WN, Montgomery JM, Garner CC. Synaptic SAP97 isoforms regulate AMPA receptor dynamics and access to presynaptic glutamate. J Neurosci. 2009; 29:4332–4345. [PubMed: 19357261]

Wenthold RJ, Petralia RS, Blahos J II, Niedzielski AS. Evidence for multiple AMPA receptor complexes in hippocampal CA1/CA2 neurons. J Neurosci. 1996; 16:1982–1989. [PubMed: 8604042]

Wyszynski M, Kim E, Dunah AW, Passafaro M, Valtschanoff JG, Serra-Pages C, Streuli M, Weinberg RJ, Sheng M. Interaction between GRIP and liprinalpha/SYD2 is required for AMPA receptor targeting. Neuron. 2002; 34:39–52. [PubMed: 11931740]

Wyszynski M, Valtschanoff JG, Naisbitt S, Dunah AW, Kim E, Standaert DG, Weinberg R, Sheng M. Association of AMPA receptors with a subset of glutamate receptor-interacting protein in vivo. J Neurosci. 1999; 19:6528–6537. [PubMed: 10414981]

Xia J, Zhang X, Staudinger J, Huganir RL. Clustering of AMPA receptors by the synaptic PDZ domain-containing protein PICK1. Neuron. 1999; 22:179–187. [PubMed: 10027300]

Xu W, Schluter OM, Steiner P, Czervionke BL, Sabatini B, Malenka RC. Molecular dissociation of the role of PSD-95 in regulating synaptic strength and LTD. Neuron. 2008; 57:248–262. [PubMed: 18215622]

Yamazaki M, Fukaya M, Abe M, Ikeno K, Kakizaki T, Watanabe M, Sakimura K. Differential palmitoylation of two mouse glutamate receptor interacting protein 1 forms with different N-terminal sequences. Neurosci Lett. 2001; 304:81–84. [PubMed: 11335060]

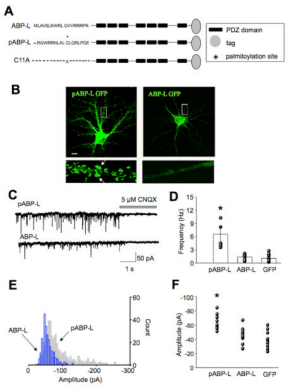

Fig. 1. Over-expression of pABP-L causes an increase in mEPSC frequency and amplitude

A, Schematic representation of isoforms of ABP. pABP-L and ABP-L differ from one another in their N-terminus 18 aa exon and the palmitoylation of the cysteine residue at position 11 in pABP-L. The C11A mutant is identical to pABP-L except the cysteine at position 11 has been replaced by an alanine. Peptides tagged at the C-terminus with GFP (ABP-L and pABP-L) of FLAG (C11A) were expressed in neurons from Sindbis virus vectors. **B,** Hippocampal neurons, 19 days in vitro (DIV19) infected with pABP-L and ABP-L respectively, for 18 hours. Scale bar 20 μm. The lower panels are magnifications of the boxed areas. pABP-L is localized preferentially in spines, as indicated by arrows. The expression of ABP-L in infected neurons is restricted to intracellular sites. **C,** Traces of mEPSCs recorded at −70mV from a pABP-L and ABP-L infected neuron at DIV 18. Downward deflections represent individual mEPSCs isolated in the presence of tetrodotoxin. CNQX was puffer-applied onto the cell for the duration indicated. **D,** Bar graph displays average frequency data from all cells, with standard error bars. *n* = 7, 9 and 12 for pABP-L, ABP-L and GFP infected neurons respectively. **E**, Amplitude histograms from a single pABP-L and ABP-L infected neuron. Note the rightward shift of the pABP-L amplitude histogram indicating the higher proportion of mEPSCs with high amplitude (gray histogram). The ABP-L histogram is confined to lower amplitudes (blue histogram). **F**, Average mEPSC amplitude data from a number of cells is displayed as a scatter graph. The mEPSC amplitude in pABP-L infected neurons was significantly different from that in ABP-L and GFP infected cells. Asterisks indicate $P < 0.05$.

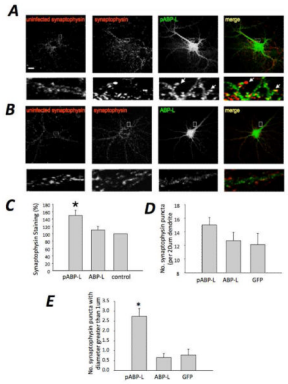

Fig. 2. Presynaptic synaptophysin staining is up-regulated by postsynaptic pABP-L expression

Hippocampal neurons at DIV 18 were fixed at 18 – 24 hours after infection with pABP-L (**A**) or ABP-L (**B**) respectively and labeled with synaptophysin antibody. Boxed regions are magnified below each image. Extreme right shows the merged GFP and synaptophysin images from an infected cell. Note the large, bright red clusters in close apposition to spines in pABP-L infected neurons (indicated with arrows in the merged image). In contrast, ABP-L infected neurons show a much lower staining for synaptophysin (lower panels. Extreme left (A, B) shows synaptophysin staining in an uninfected neuron close to an infected neuron. Scale bar = 20 μm. **C**, Bar graphs showing synaptophysin staining in pABP-L expressing neurons was significantly greater ($p<0.05$) than in ABP-L infected neurons (expressed as a percentage of control). **D,** Bar graphs showing the number of synaptophysin puncta (per 20 μm dendrite) contacting infected cells were not significantly different between pABP-L, ABP-L and GFP infected cells. **E,** Bar graphs showing a greater number of synaptophysin puncta with a diameter of more than 1 μm were observed in pABP-L infected cells ($p<0.05$) than ABP-L or GFP infected neurons.

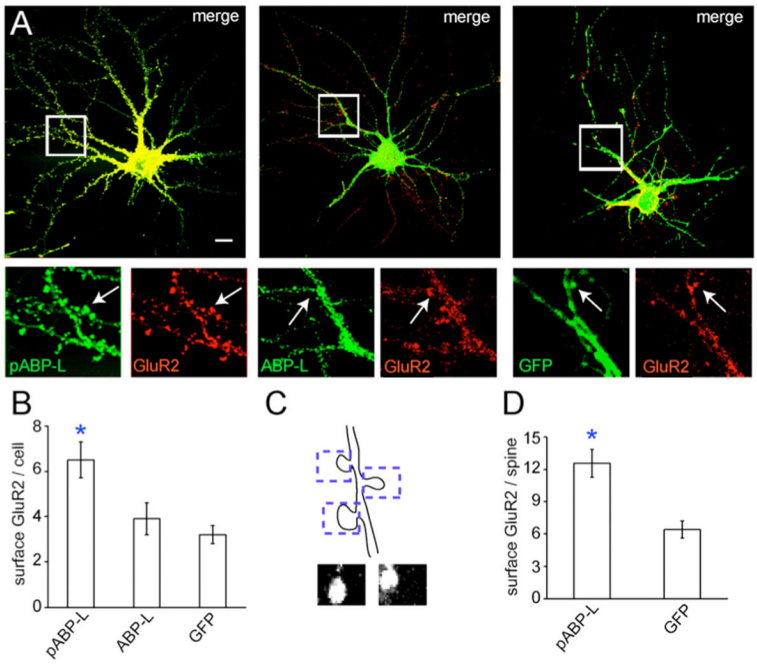

Fig. 3. Surface GluR2 levels increase in pABP-L overexpressing neurons

A, Hippocampal neurons infected at DIV 18 with pABP-L, ABP-L and GFP respectively. 18 – 24 hours after infection fixed, but not permeabilized, neurons were labeled with monoclonal GluR2 N-terminal antibody to visualize endogenous surface GluR2. Boxed regions are magnified below the merged image. Clear co-localization of pABP-L (green) and GluR2 (red) was observed in spines (indicated with arrows in the left hand panels). In contrast only GluR2 was detected in spines in ABP-L infected cells (middle panels, arrows). GluR2 co-localized with GFP (right panels), though the intensity of GluR2 staining was reduced when compared with pABP-L expressing cells. **B,** Bar graph of average data from a number of cells (n = 3; 17 cells), quantifying the levels of endogenous surface GluR2 in pABP-L, ABP-L and GFP infected neurons (arbitrary units). Asterisks indicate significantly different from control and ABP-L; $P < 0.05$. **C,** Schematic depicting the isolation of individual spines for quantitation. A 2 μm by 4 μm box isolated the spine and the level of GluR2 within this region was quantified. Lower images show two individual spines 'dissected' in this way. **D,** Bar graph showing mean endogenous surface GluR2 levels within individual spines in pABP-L (n = 17; 97 spines) and GFP (n =14; 40 spines) infected neurons (arbitrary units). Asterisks indicate significant difference from GFP expressing cells ($P<0.05$).

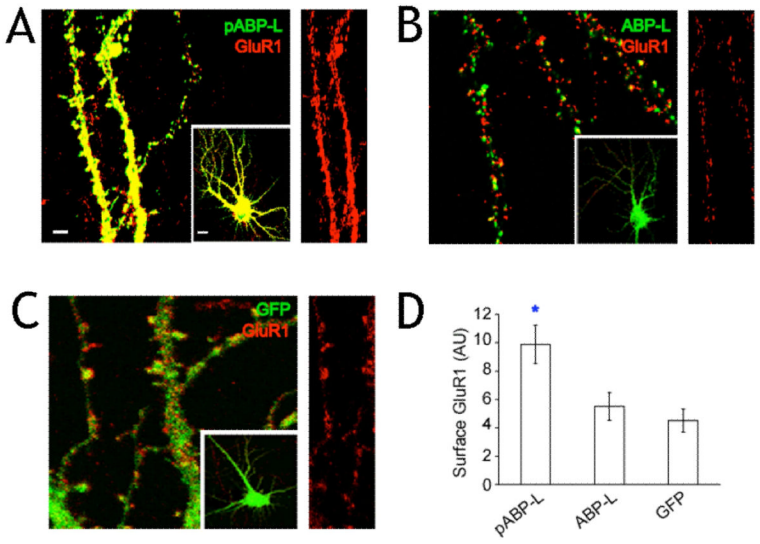

Fig. 4. Surface levels of endogenous GluR1increase in pABP-L expressing neurons.

Immunostaining of neurons infected with Sindbis virus expressing **A,** pABP-L **B,** ABP-L and **C,** GFP alone. 18-24 hours after infection, fixed (but not permeabilized) neurons were labeled with a polyclonal GluR1 N-terminal antibody to visualize endogenous surface GluR1. Magnified images of infected dendrites (scale bar = 3 μm) are shown from the infected cells in the inset (scale bar = 10 μm). Right hand panel of each image shows endogenous surface GluR1 staining in isolation for comparison. **D,** Quantitation of endogenous surface GluR1 staining in infected neurons (*n* = 20 cells; 3 experiments). Asterisk indicates significant difference from ABP-L and GFP ($P<0.01$). AU = arbitrary units.

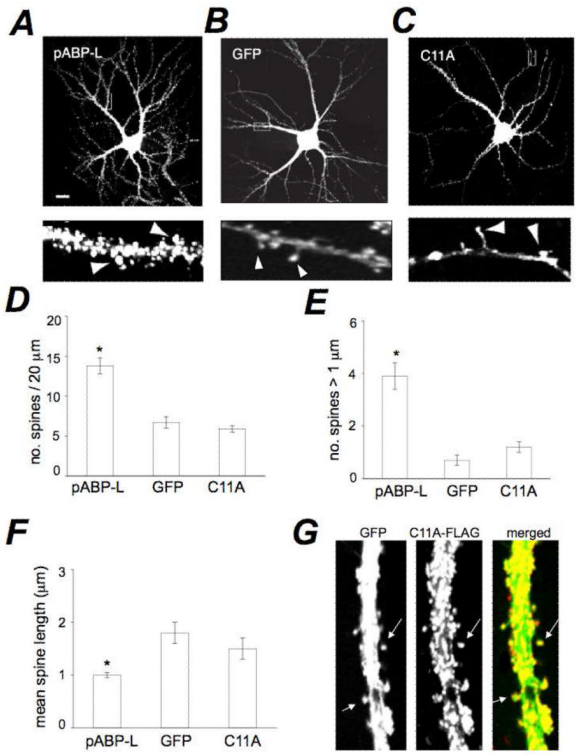

Fig. 5. Expression of pABP-L enhances spine size and number

Hippocampal neurons at DIV 19 infected with sindbis virus expressing (**A**) pABP-L, (**B**) GFP or (**C**) the pABL-L mutant, C11A. Scale bar = 10 µm. Lower panels are 20 µm magnifications of dendrites from the cell shown. Note presence of large spines lacking shanks in pABP-L expressing neurons (indicated with arrowheads) and spines with small heads at the end of filamentous structures in GFP infected cells. **D**, **E**, **F**, Bar graphs depicting the noted spine parameters in pABP-L, GFP and C11A expressing neurons, respectively. The density of spines increased in pABP-L expressing neurons relative to GFP or C11A expressing neurons (**D**) (n = 3, 18 cells; * $P < 0.001$). The number of spines greater than 1 µm in diameter was also significantly greater in pABP-L infected neurons (**E**) (* $P<0.05$). GFP and C11A expressing cells displayed spines with a greater length when compared with pABP-L infected cells (**F**) (*$P < 0.05$). **G**, Dendrite of neuron co-expressing GFP and the C11A mutant, both from sindbis viral vectors. HA-tagged C11A (red) and GFP (green) were detected by immune fluorescence.

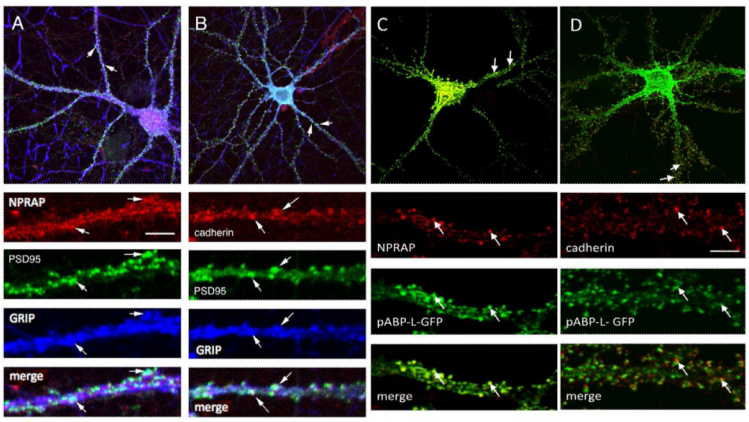

Fig. 6. ABP and GRIP colocalize with NPRAP and cadherin at synapses

The designated proteins were localized in dissociated embryonic hippocampal neurons 19–21 DIV in culture by immunofluorescence as described in Experimental Methods. **A**, Endogenous NPRAP colocalizes with endogenous GRIP at synapses, stained with a postsynaptic marker, PSD95. **B**, Endogenous cadherin colocalizes with endogenous GRIP at synapses, stained with a postsynaptic marker, PSD95. **C**, Sindbis expressed pABP-LGFP colocalizes with endogenous NPRAP and **D**, Sindbis expressed pABP-L-GFP colocalizes with endogenous cadherin. Arrows identify sites of protein colocalization. Scale bars: Top panels, 10 μm; bottom panels, 3 μm.